I&EC research
Industrial & Engineering Chemistry Research
pubs.acs.org/IECR
Article

Formation Energetics and Guest—Host Interactions of Molybdenum Carbide Confined in Zeolite Y

Xianghui Zhang, Margaret E. Reece, Cody B. Cockreham, Hui Sun, Baodong Wang, Hongwu Xu, Junming Sun, Xiaofeng Guo, Ha Su, Yong Wang, and Di Wu*

Cite This: *Ind. Eng. Chem. Res.* 2021, 60, 13991−14003

Read Online

ACCESS | Metrics & More | Article Recommendations | Supporting Information

ABSTRACT: Once confined in zeolites, carbides of inexpensive transition metals, such as molybdenum (Mo) and tungsten (W), exhibit similar catalytic activity as platinum group noble metals. Thus far, the intrinsic thermodynamic properties and their relations with the local interfacial phenomena of such carbide−zeolite heterogeneous catalytic materials have rarely been explored. Here, employing high temperature oxide melt solution calorimetry, for the first time, we determined the energetics of molybdenum carbide (Mo_2C) formation under confinement in zeolite Y (Mo_2C/FAU) as a function of Si/Al ratio experimentally. As Si/Al ratio increases, the formation enthalpies of Mo_2C/FAU from constituent oxides and carbides become less endothermic, spanning within a narrow range, between ∼0 and 10 kJ/mol TO_2 (tetrahedron unit). Confinement of refractory Mo_2C in zeolite Y is energetically more favorable than encapsulation of MoO_3 in the same host, by more than ∼30 kJ/mol TO_2. Such significant energetic differences between Mo_2C/FAU and MoO_3/FAU in formation enthalpies and the highly exothermic Mo_2C−FAU guest−host interaction energies, highlight robust bonding at the carbide−zeolite interfaces that harnesses the refractory nature of Mo_2C guest species, and compensate the energetic deficiency for achieving subnano-sized Mo_2C particles.

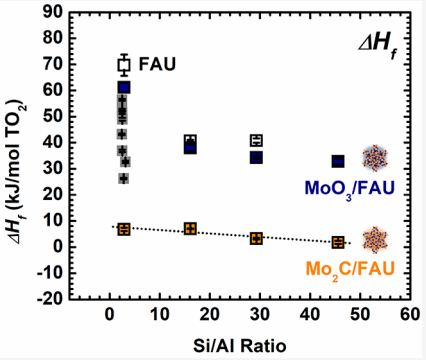

INTRODUCTION

Zeolite-based heterogeneous catalytic materials play critical roles in multiple fields of modern chemical industry. Examples include selective conversion of fossil fuels,[1,2] biomass conversion, and biorefinery.[3−5] In these applications, noble metal nano- or subnano-particles encapsulated in zeolites show high performance, yet development of stable alternative catalytic materials using earth-abundant elements is necessary for a more sustainable future. It has been reported that once properly supported, refractory carbides of inexpensive major industrial metals, such as molybdenum (Mo) and tungsten (W), present comparable activity as platinum (Pt) group noble metals.[6,7] For instance, encapsulation of Mo and W carbides in zeolites, such as ZSM-5 and zeolite Y, leads to catalysts with high stability and comparable performance as the noble metal−zeolite systems in biomass[8,9] and crude oil[10,11] upgrading, and methane dehydroaromatization.[12,13] Encapsulation in zeolite frameworks enables "sinter-proof", dispersed transition metal carbide (TMC) particles with uniform size, and high catalytic activity, selectivity, and stability. Moreover, the crystalline zeolite framework with well-defined porosity can tolerate the tough carbide synthesis conditions. Current research focusing on TMC/zeolite catalysts is rich in reaction kinetics and pathway design, and activity/selectivity boost.[14,15] Several computational thermodynamic predictions have been documented.[16,17] However, there is few experimental study on the formation energetics of TMC/zeolite systems, which governs the bonding specifics of guest−host interfaces and stabilizes the highly metastable subnano-sized TMC particles/clusters. Such quantitative energetic insights will enable benchmarking data for machine learning and simulation for predictive design, synthesis, and process of TMC−zeolite catalytic materials.

The thermochemistry of zeolites has been pioneered by Prof. Alexandra Navrotsky and collaborators over the past a few decades, in which formation of zeolite pure phases,[18−26] and small molecule−zeolite binding (water, CO_2, and small organics)[27−31] have been systematically studied. A comprehensive review can be found in the references.[20] However, as mentioned earlier, we realize that the potentially rich energetic landscape, and guest−host interactions for zeolite-encapsulation of TM-based solid-state materials with much higher melting points, such as oxides (TMOs), carbides (TMCs) and nitrides (TMNs), have not been systematically explored. Our recent research on confinement/encapsulation of heterocore particles is primarily on the TMO−aluminosilicate zeolite

Received: July 15, 2021
Published: September 17, 2021

Downloaded via UNIV OF CALIFORNIA DAVIS on September 29, 2021 at 08:20:24 (UTC).
See https://pubs.acs.org/sharingguidelines for options on how to legitimately share published articles.

ACS Publications
© 2021 American Chemical Society

https://doi.org/10.1021/acs.iecr.1c02822
Ind. Eng. Chem. Res. 2021, 60, 13991−14003

systems.[32,33] Owing to their negatively charged microporous frameworks constructed by corner-sharing tetrahedra (TO_4, T = Si^{4+} or Al^{3+}), aluminosilicate zeolites are friendly hosts welcoming guest species with proper sizes, ranging from water to small organics and cations. Such an open system with tunable surfaces and compositions enables intricate local chemistry within the pores which defines the nature of the guest species, and determines the strength of guest−host interactions. Recently, using adsorption calorimetry, we determined the formation energetics of copper oxo clusters (CuO_x) under tight confinement of mordenite (MOR) with water as the gentle oxidant in real-time.[32] Meanwhile, hydration thermodynamics of other TM-MOR samples, including Co- and Fe-MOR, was investigated. Our results highlighted the high thermal stability of CuO_x in MOR, up to 915 °C in nitrogen flow, compared with other guest species such as iron carbonates and/or bicarbonates detected in Fe-MOR. Meanwhile, we elucidated the critical roles of small molecular species, such as water and CO_2, in minimizing the overall energy of the TMO−zeolite systems by effective stabilization of ionic species.[34] Very recently, we investigated the thermodynamics of molybdenum trioxide (MoO_3) particles encapsulated in zeolite Y (faujasite or FAU) with varied Si/Al ratio.[33] Interestingly, we found that encapsulation of MoO_3 only slightly neutralized the metastability of zeolite Y, which has an endothermic formation enthalpy compared with constituent oxides (SiO_2, Al_2O_3, and H_2O). Additionally, at the same MoO_3 loading, higher framework Si/Al ratio resulted in less endothermic MoO_3/FAU formation enthalpies, ranging from 61.1 ± 1.8 kJ/mol TO_2 at Si/Al = 2.9 to 32.8 ± 1.4 kJ/mol TO_2 at Si/Al = 45.6. These studies strongly suggest that the encapsulation thermodynamics of TMOs in zeolites is closely governed by the Si/Al ratio, and the chemical natures of the TMO guest species. Moreover, we also noticed that once present as the guests in zeolite frameworks, TMOs appear to be "flexible" taking advantage of the confinement chemistry and other guest species, such as water and CO_2 to alter their chemical identity, phases, oxidation states and/or local structures, seeking for the lowest possible energetic states under encapsulation.

Here, we report the first experimental thermodynamic (calorimetric) study on the confinement of molybdenum carbide in zeolite Y (Mo_2C/FAU) with a wide range of Si/Al ratios, from 2.9 to 45.6. Zeolite Y is selected as the host candidate to sustain the harsh synthesis conditions of refractory TMCs involving a carburization process at temperatures about 700 °C. Employing the unique calorimetric capabilities in the Alexandra Navrotsky Institute for Experimental Thermodynamics (AlexInstitute) at Washington State University (WSU) with supports from structural, morphological, *in situ* spectroscopic, and integrated thermal analyses, we revealed the formation energy landscape of Mo_2C/FAU as Si/Al ratio varies, elucidated the energetically favorable Mo_2C−FAU guest−host interactions, and compared the distinctively different thermodynamics of Mo_2C encapsulation with MoO_3 confinement in FAU.

EXPERIMENTAL METHODS

Material Synthesis. Zeolite HY samples with different Si/Al ratios, from 2.9 to 45.6, were obtained from Alfa Aesar. These samples were also used in our earlier study on thermodynamics of MoO_3 encapsulated in zeolite Y.[33] Synthesis of materials with molybdate carbides confined in zeolite HY (Mo_2C/FAU) has three steps, including (1) Mo precursor introduction via impregnation, (2) Mo oxide formation in FAU (MoO_3/FAU) by calcination in air, and (3) carburization of MoO_3 to form Mo_2C in FAU. Specifically, by incipient wetness impregnation (IWI) of ammonium molybdate tetrahydrate (AMT, Sigma-Aldrich, 99%), the same amount of Mo precursor, was loaded into the void space of each FAU to ensure all samples have the same Mo content of 5 wt %. After pretreatment at 80 °C under vacuum for at least 4 h, the FAU sample (1.0 g) was impregnated with aqueous solution of AMT (1.5 mL, 0.05 mol/L). Subsequently, the impregnated FAU was sonicated for 1 h in ambient conditions followed by oven-drying at 120 °C for at least 12 h before oxidative calcination at 600 °C in air for 10 h in a furnace leading to the formation of MoO_3/FAU. Eventually, MoO_3/FAU was carburized under 15 vol % CH_4/H_2 flow (85 mL/min) for the final product, Mo_2C/FAU. More specifically, according to Iida et al.,[8] under continuous 15 vol % CH_4/H_2 flow of 85 mL/min, the furnace temperature was increased stepwise, to 300 °C at 5 °C/min first, and to 700 °C at 1 °C/min followed by isothermal treatment at 700 °C for at least 2 h for complete carburization. The dominant molybdenum carbide phase in FAU is Mo_2C according to previous reports.[35,36] The sample labeled as Mo_2C/2.9FAU represents Mo_2C confined/encapsulated in zeolite Y (FAU) with a Si/Al ratio of 2.9.

Sample Characterizations. The composition of each sample was determined by coupling inductively coupled plasma mass spectrometry (ICP-MS, Agilent 770) and thermal analysis using an integrated thermogravimetry−differential scanning calorimetry−mass spectrometry system (TG-DSC-MS, Netzsch STA 449 F5 Jupiter integrated QMS 403 D Aëolos). In a measurement, the sample powder was placed in a platinum (Pt) crucible prior to analysis from 30 to 1000 °C (10 °C/min) in N_2 flow (50 mL/min). The evolved species in TG-DSC were simultaneously analyzed by a mass spectrometer (MS) coupled with a heated (200 °C) capillary to identify the chemical nature and amount of desorbed and/or decomposed species. The dehydration enthalpies at 25 °C were also calculated based on the TG-DSC-MS data.

Powder X-ray diffraction (XRD) was performed on each sample at room temperature employing a Rigaku Miniflex 600 diffractometer (40 kV, 15 mA, Cu Kα, λ = 1.5406 Å). Data was collected between 5 and 60° at 2°/min. N_2 adsorption−desorption full isotherm analysis was carried out on each sample at −196 °C using a Micromeritics 3Flex multiport analyzer, in which the sample was outgassed at 300 °C under vacuum for at least 5 h before each measurement. The isotherm data collected were used to derive the Brunauer−Emmett−Teller (BET) surface area and pore size distribution. Transmission electron microscopy (TEM) was employed to evaluate the sample morphology by using a FEI Tecnai T20 instrument with LaB_6 cathode at 200 kV. Specifically, a small amount of specimen was suspended via ultrasonication in ethanol. The obtained suspension was dropwise introduced on a 200-mesh carbon-coated nickel grid followed by drying under an infrared lamp for 20 min.

Ex situ diffuse reflectance infrared Fourier transform spectroscopy (DRIFTS, Nicolet iS50, Thermo Scientific) was conducted on each sample. Specifically, 25 mg of sample was loaded in the DRIFTS cell, and spectra were collected at room temperature between 4000 and 650 cm^{-1}. *In situ* DRIFTS experiments during CO adsorption−desorption were carried

https://doi.org/10.1021/acs.iecr.1c02822
Ind. Eng. Chem. Res. 2021, 60, 13991−14003

Table 1. Compositional, Structural and Surface Properties of All Samples Studied, Including the Parent FAU,[33] Intermediate Phase MoO_3/FAU,[33] and the Final Carburization Product Mo_2C/FAU. All Data on FAU and MoO_3/FAU Were Referenced from Our Earlier Report[33]

sample	chemical composition on TO_2 Basis	MW	a (Å)	BET surface area (m^2/g)	specific volume (m^3/g)	pore size (nm)
2.9FAU	$(SiO_2)_{0.742}$ $(Al_2O_3)_{0.13}$·$0.916H_2O$[33]	74.23[33]	8.2906[33]	1067.4[33]	0.65[33]	0.72[33]
16.1FAU	$(SiO_2)_{0.942}$ $(Al_2O_3)_{0.03}$·$0.196H_2O$[33]	63.07[33]	8.0297[33]	1176.4[33]	0.79[33]	0.77[33]
29.3FAU	$(SiO_2)_{0.967}$ $(Al_2O_3)_{0.017}$·$0.136H_2O$[33]	62.23[33]	8.0424[33]	1203.9[33]	0.72[33]	0.78[33]
45.6FAU	$(SiO_2)_{0.979}$ $(Al_2O_3)_{0.011}$·$0.078H_2O$[33]	61.28[33]	8.145[33]	911.1[33]	0.58[33]	0.78[33]
MoO_3/2.9FAU	$(MoO_3)_{0.025}$ $(SiO_2)_{0.742}$ $(Al_2O_3)_{0.13}$·$0.727H_2O$[33]	74.37[33]	8.1581[33]	703.1[33]	0.44[33]	0.72[33]
MoO_3/16.1FAU	$(MoO_3)_{0.031}$ $(SiO_2)_{0.942}$ $(Al_2O_3)_{0.03}$·$0.177H_2O$[33]	67.24[33]	7.9671[33]	631.6[33]	0.46[33]	0.76[33]
MoO_3/29.3FAU	$(MoO_3)_{0.027}$ $(SiO_2)_{0.967}$ $(Al_2O_3)_{0.017}$·$0.138H_2O$[33]	66.15[33]	8.0297[33]	1057.2[33]	0.65[33]	0.77[33]
MoO_3/45.6FAU	$(MoO_3)_{0.027}$ $(SiO_2)_{0.979}$ $(Al_2O_3)_{0.011}$·$0.120H_2O$[33]	65.91[33]	8.0424[33]	631.6[33]	0.43[33]	0.77[33]
Mo_2C/2.9FAU	$(MoC_{0.5})_{0.025}$ $(SiO_2)_{0.742}$ $(Al_2O_3)_{0.13}$·$0.540H_2O$	70.21	8.11	581.1	0.35	0.72
Mo_2C/16.1FAU	$(MoC_{0.5})_{0.031}$ $(SiO_2)_{0.942}$ $(Al_2O_3)_{0.03}$·$0.137H_2O$	65.39	8.15	530.7	0.39	0.76
Mo_2C/29.3FAU	$(MoC_{0.5})_{0.027}$ $(SiO_2)_{0.967}$ $(Al_2O_3)_{0.017}$·$0.105H_2O$	64.57	8.12	715.1	0.45	0.78
Mo_2C/45.6FAU	$(MoC_{0.5})_{0.027}$ $(SiO_2)_{0.979}$ $(Al_2O_3)_{0.011}$·$0.102H_2O$	64.64	8.11	777.4	0.50	0.77

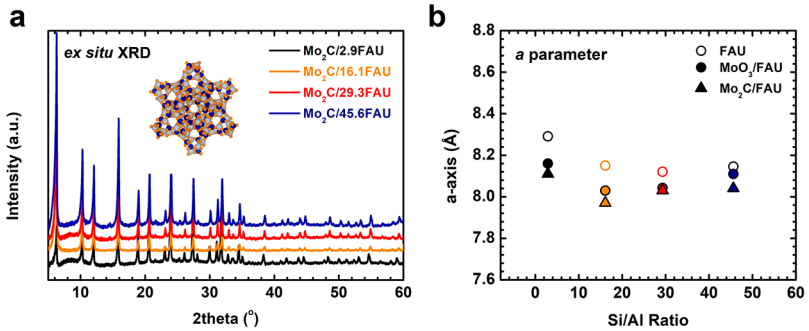

Figure 1. (a) Room temperature *ex situ* XRD patterns of Mo_2C/FAU with the schematic illustration of FAU included, and (b) lattice parameter, a, of all Mo_2C/FAU samples as Si/Al ratio increases from 2.9 to 45.6. The a parameters of FAU and MoO_3/FAU we reported earlier are also included for comparison.[33]

out on each sample in a high temperature cell (Spectra-Tech) equipped with ZnSe windows. Before spectrum collection, the sample was pretreated at 600 °C under H_2/He flow (10 vol %, 45 mL/min) for half an hour to remove adsorbed species. Subsequently, the cell was cooled down to 35 °C, and the gas stream was switched to pure He with the same flow rate for background spectrum recording. The gas flow was switched from He to pure CO for real-time collection of adsorption spectra every 5 min until CO adsorption saturation. In desorption, the spectra were collected under pure He flow every 5 min. If CO could not be completely removed at 35 °C by He flow, the desorption temperature would be increased to 50 °C to ensure complete CO desorption.

Calorimetry. High temperature oxide melt drop solution calorimetry experiments were carried out using a Tian-Calvet twin calorimeter (Setaram Alexsys-1000) in the Nuclear Science Center (NSC) at WSU. The detailed approach of this methodology was described elsewhere by Navrotsky et al.[37] Typically, this calorimetric methodology is employed for direct measurement of heat of reaction, including the sum of heat content of the sample and its dissolution heat and/or any other potential reactions at the solvent temperature. Using the heats of reaction obtained, we are able to derive the enthalpies of formation of materials at room temperature. More specifically, in each measurement, about 5 mg of sample was pelletized and directly dropped into the calorimeter that hosts lead borate ($2PbO·B_2O_3$) molten salt at 700 °C as the solvent under air flow of 120 mL/min. Calibration of the calorimeter was performed by measuring the heat content of Al_2O_3 (corundum). Measurements on the same sample were repeated for at least four times to ensure reproducibility. The directly quantified enthalpies of dissolution (ΔH_{ds}) were applied to derive the formation enthalpies (ΔH_f) from constituent oxides and Mo_2C, and elements ($\Delta H_{f,el}$), and to estimate the guest−host interactions between Mo_2C and zeolite Y using a thermodynamic cycle. Errors were calculated as two standard deviations of the mean.

RESULTS AND DISCUSSION

According to the ICP-MS data, we determined the compositions of all Mo_2C/FAU samples (see Table 1). We also listed the compositional data of FAU and MoO_3/FAU for comparison.[33] The water content of each sample was quantified based on the dehydration weight loss (%) from TG and MS. As expected, the general trend is that as Si is enriched, the degree of hydration of Mo_2C/FAU sample decreases.

Room temperature *ex situ* powder XRD patterns confirm that the FAU frameworks of all Mo_2C/FAU samples retain cubic structures ($Fd3m$) after harsh carburization at 700 °C (see Figure 1a). Notably, there is no observable XRD peak corresponding to bulk β-Mo_2C, which is a clear evidence suggesting that the FAU-encapsulated Mo_2C particles are well dispersed within the internal void space of zeolite Y (see Figure S1 for the XRD patterns of bulk β-Mo_2C). The lattice parameters a of FAU, MoO_3/FAU, and Mo_2C/FAU samples are listed in Table 1, and plotted in Figure 1b. As Si/Al ratio

https://doi.org/10.1021/acs.iecr.1c02822
Ind. Eng. Chem. Res. 2021, 60, 13991−14003

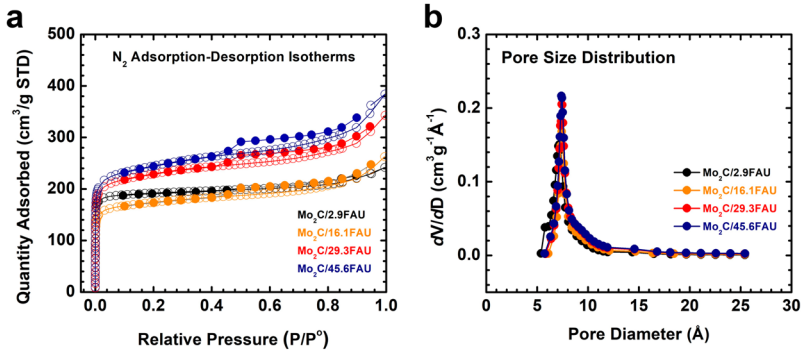

Figure 2. (a) N_2 adsorption−desorption isotherms at −196 °C and (b) pore size distribution plots of all Mo_2C/FAU samples.

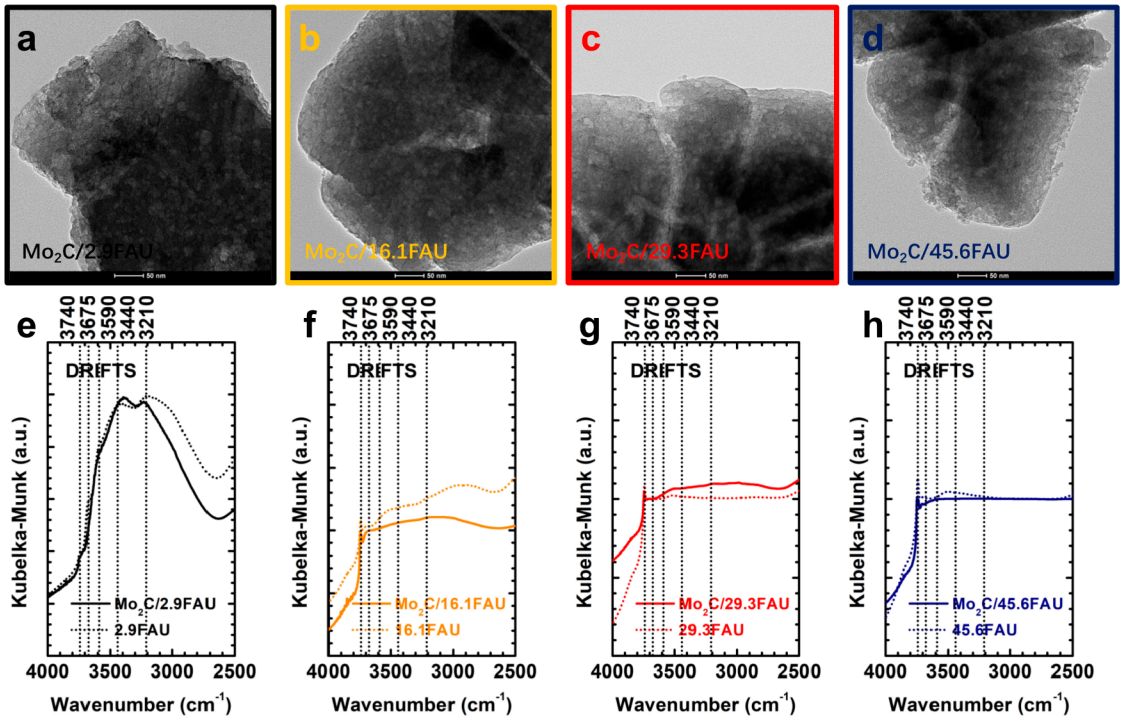

Figure 3. (a−d) TEM images, and (e−h) *ex situ* DRIFTS data of all Mo_2C/FAU samples. Sample names are labeled in each figure. The spectra of the parent FAU samples reported earlier are also plotted for comparison.[33]

increases, decreasing *a* parameters were seen on each group of samples, FAU, MoO_3/FAU, or Mo_2C/FAU. Meanwhile, at the same Si/Al ratio, the *a* parameter decreases following the rank of FAU, MoO_3/FAU, and Mo_2C/FAU. In other words, high temperature carburization of MoO_3/FAU for Mo_2C/FAU results in decreased lattice dimension.

The specific area of each Mo_2C/FAU sample was determined by N_2 adsorption−desorption isotherm (−196 °C) data using the BET method (see Figure 2a). Carburization leads to surface area decreases by roughly 20%. Specifically, the surface areas are 581.1 m^2/g for Mo_2C/2.9FAU, 530.7 m^2/g for Mo_2C/16.1FAU, 715.1 m^2/g for Mo_2C/29.3FAU, and 777.4 m^2/g for Mo_2C/45.6FAU. On the other hand, the pore size distribution plots in Figure 2b suggest that all Mo_2C/FAU samples share uniform micropores of ∼0.8 nm, approximately the same as those of FAU and MoO_3/FAU (Table 1). This phenomenon confirms the structural and thermal stability of FAU as the host framework for synthesis particles/clusters of refractory materials and high temperature ceramics. In addition, the TEM images suggest that after carburization at 700 °C each Mo_2C/FAU retains its general morphology, particle size (400−600 nm), and interconnected nanoscale porosity (see Figure 3a−d). Under the current TEM resolution, the encapsulated Mo_2C particles are not easily observed because they are too light to generate the contrast under the electron beam, and the absence of detectable bulk Mo_2C chunks on the external surface of FAU indicates dispersed Mo_2C clusters under internal micropore confinement.

Ex situ DRIFTS experiments were carried out to elucidate the interfacial bonding evolutions of FAU upon Mo_2C encapsulation (Figure 3e−h). The full range DRIFTS data are presented as Figure S2. As Si is enriched, the framework hydrophobicity is enhanced, leading to decreased intensity for the bending vibration of water at 1640 cm^{-1} (Figure S2). Similarly, encapsulation of Mo_2C also results in decreased hydroxyl concentration, seen for both silanols (Si−OH) and aluminols (Al−OH), and adsorbed water. More specifically, Mo_2C confinement in 2.9FAU, the sample with the highest Al content, decreases the intensities of (i) shoulder peaks at 3675

https://doi.org/10.1021/acs.iecr.1c02822
Ind. Eng. Chem. Res. 2021, 60, 13991−14003

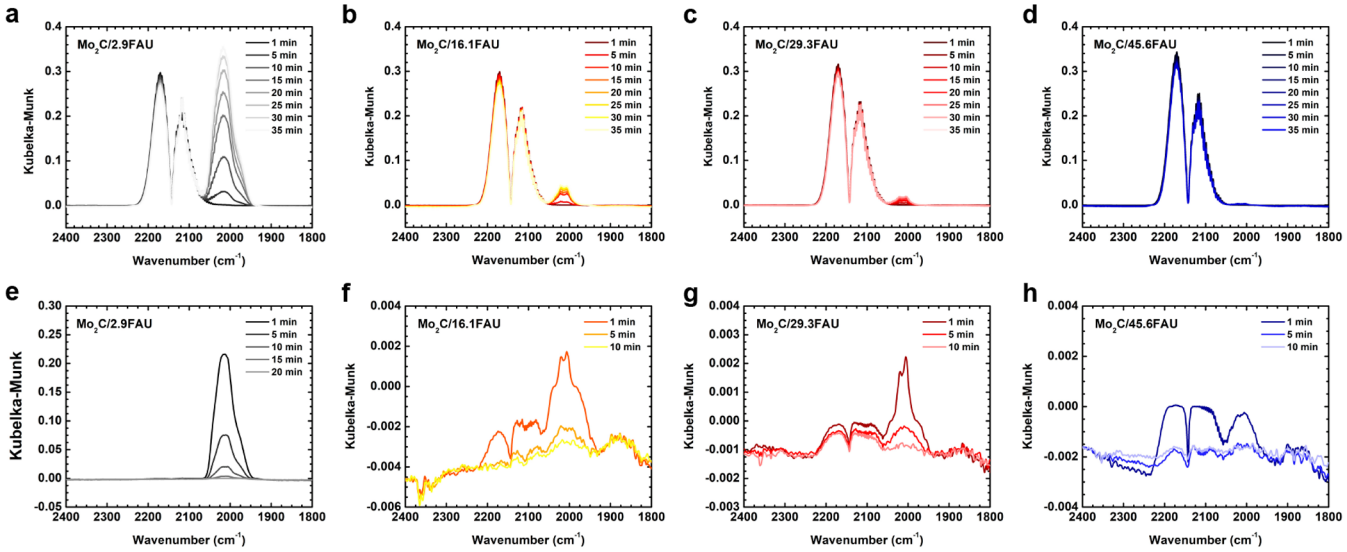

Figure 4. *In situ* DRIFTS data of all Mo_2C/FAU samples in CO (a–d) adsorption and (e–h) desorption. Sample names are labeled in each figure.

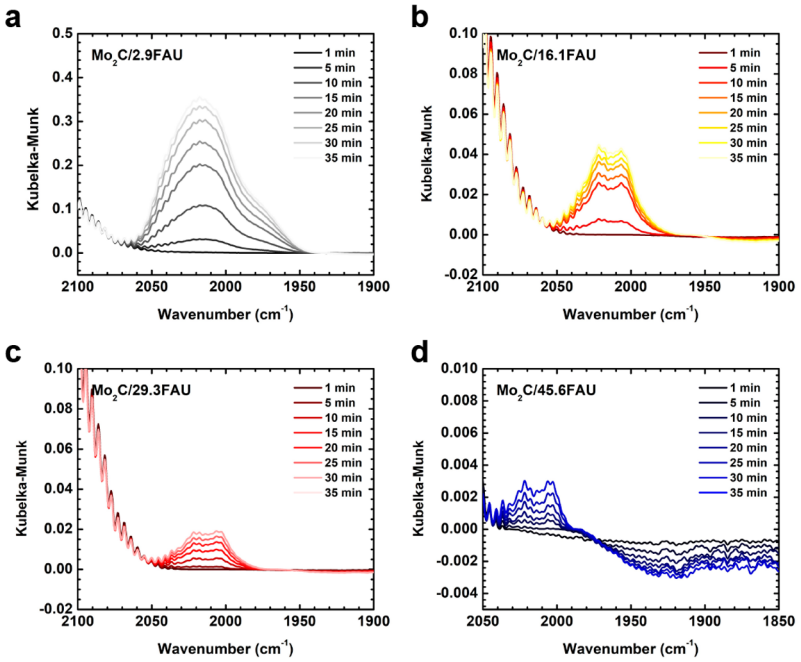

Figure 5. *In situ* DRIFTS data of all Mo_2C/FAU samples in CO adsorption with the evolving peaks highlighted. (a) Mo_2C/2.9FAU, (b) Mo_2C/16.1FAU, (c) Mo_2C/29.3FAU, and (d) Mo_2C/45.6FAU.

and 3590 cm^{-1} belonging to the stretching vibration of O–H bond of Brønsted acid sites,[17,32,38] and (ii) peaks at 1640 cm^{-1} from bending vibration of H_2O molecules (Figure S2a). For FAU frameworks with higher Si content (Si/Al = 16.1, 29.3 and 45.6), Mo_2C is primarily anchored at the silanols (Si–OH),[17,33,38] resulting in decreased intensity at 3740 cm^{-1} attributed to isolated silanols.[39,40] In other words, the binding locations of MoO_3 particles likely determine the anchoring sites of Mo_2C clusters. Thus, for the Al-rich FAU (2.9FAU), MoO_3 and Mo_2C selectively favor the Brønsted acid sites by the Al atom. As the Si content increases, a full range of silanols begin to play dominant roles serving as the major binding sites for MoO_3 and Mo_2C clusters in FAU. Moreover, this set of *ex situ* DRIFTS data indicates that carburization of MoO_3 for Mo_2C formation under FAU confinement leads to recovery of silanols (3740 cm^{-1}). Indeed, formation of Mo_2C under CH_4/H_2 flow is associated with (i) MoO_3–FAU bond breaking, (ii) formation of water, and/or (iii) restoration of framework hydroxyl groups.[13,41] These simultaneous reactions result in sintered Mo_2C clusters with size growth.[12,42,43] According to our *ex situ* DRIFTS results, hydroxyl restoration and Mo_2C sintering are particularly common for Mo_2C/FAU when Si/Al is higher than 16.1. This is perhaps due to the weaker MoO_3/Mo_2C–FAU guest–host interactions at the silanols (Si–OH) compared with the binding at the aluminols (Al–OH) or Brønsted acid sites. We anticipate that such differences in interfacial bonding strength as a function of Si/Al ratio will be probed by calorimetry and reflected by the formation enthalpies of Mo_2C/FAU and the Mo_2C–FAU interaction energies.

https://doi.org/10.1021/acs.iecr.1c02822
Ind. Eng. Chem. Res. 2021, 60, 13991–14003

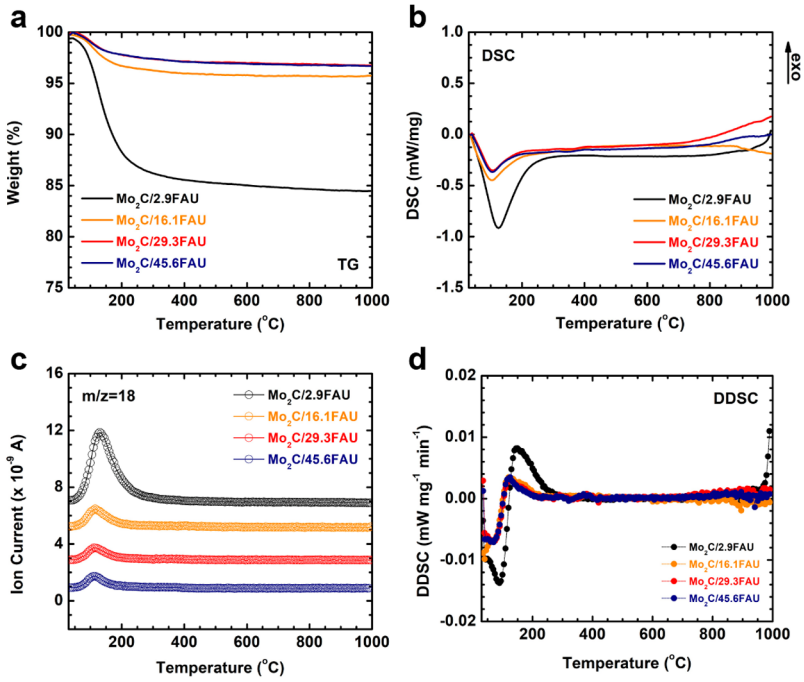

Figure 6. Thermal analysis results of Mo_2C/FAU samples. (a) TG, (b) DSC, (c) MS (m/z = 18), and (d) DDSC with N_2 flow at 50 mL/min from 30 to 1000 °C.

The influence of framework Si/Al ratio on the electron density and dispersion of Mo_2C particles was probed by *in situ* DRIFTS of CO adsorption (see Figure 4). Generally, two types of direct information are obtained from *in situ* DRIFTS of CO adsorption. Specifically, (i) the number of CO binding sites, which reflects the degree of dispersion of electron donating particles, is proportional to the intensity of adsorbed CO; (ii) the strength of CO−surface site interactions is reflected by the position (frequency) of the peak. In Figure 4, for all Mo_2C/FAU samples, there are three major peaks, at 2170, 2120, and 2020 cm^{-1}, that evolve consistently in the CO adsorption process. The peaks at 2170 and 2120 cm^{-1} belong to the vibration of gas phase CO, which we will not discuss beyond this point. The peak at 2020 cm^{-1} is attributed to adsorbed CO, the intensity of which experiences significant changes as a function of Si/Al ratio. Specifically, an abrupt decrease in its intensity is observed, from 0.35 to 0.05, as the Si/Al ratio of FAU increases from 2.9 to 16.1. Further Si content increase leads to nearly negligible CO signal. In other words, the number of well-dispersed Mo_2C particles with CO-accessible surfaces decreases as a function of Si/Al ratio. Hence, considering all samples share the same Mo_2C loading, it is clear that the degree of Mo_2C dispersion decreases with increasing Si/Al ratio.

On the other hand, the frequency of adsorbed CO also shifts as the FAU Si/Al ratio increases. Particularly, CO adsorption on Mo_2C/2.9FAU results in a symmetric peak centered at 2020 cm^{-1}, which is also clearly observed during CO desorption (see Figure 4e). For Mo_2C/16.1FAU, Mo_2C/29.3FAU, and Mo_2C/45.6FAU, CO adsorption generates a pair of peaks at 2007 and 2020 cm^{-1}. According to a report on Mo_2C/Al_2O_3 by Wu et al.,[44] the peak at 2020 cm^{-1} is attributed to the stretching vibration of CO adsorbed on $Mo^{\delta+}$ (δ = 0−2). They considered that the peak at 2007 cm^{-1} is probably due to CO binding at partially reduced Mo. Therefore, *in situ* DRIFTS of CO adsorption−desorption results suggest strong Mo_2C−FAU interactions mainly at the Al−OH sites which ensure the formation of well-dispersed Mo_2C particles under encapsulation of the Al-rich 2.9FAU. This type of binding has high polarity because of the significantly charged FAU framework. In contrast, as Si/Al increases, the relatively weak Mo_2C−FAU bindings primarily at a series of Si−OH groups dominate, governing formation of Mo_2C particles with less uniform distribution with partial Mo reduction. In the latter case, the Mo_2C−FAU interactions feature more covalent factors. We also expect such interfacial binding variations would be mirrored by the thermochemically derived enthalpies of Mo_2C−FAU guest−host interactions.

The thermal analysis data, including TG, DSC, MS, and DDSC (derivative differential scanning calorimetry) are presented in Figure 6. We also plotted the DTG (derivative thermogravimetry) traces in Figure S3. The TG traces are fairly straightforward, in which each Mo_2C/FAU presents a single-step dehydration lasting from room temperature to about 300 °C. Specifically, Mo_2C/2.9FAU has the highest degree of hydration of 15.5 wt %, while all the other samples with higher Si contents have lower degree of hydration (Figure 6a). On the basis of the TG-DSC curves, we derived the dehydration enthalpies ($\Delta H_{del,l}$) of all Mo_2C/FAU samples (see Table S2). Unlike the MoO_3 particles confined in FAU, which exhibit complex phase and/or redox evolutions as we reported in an earlier study,[33] the DSC and DDSC curves of encapsulated Mo_2C are nearly "featureless", and do not show any calorimetrically detectable events between 300 and 800 °C. In addition, the evolving DSC profiles between 800 and 1000 °C reflect framework amorphization to energetically more stable high temperature amorphous phases, evidenced by the post thermal analysis *ex situ* XRD data (see Figure S4). Indeed, because of the intrinsic high melting point of Mo_2C (2687 °C), melting point depression of confined Mo_2C guest species was not observed within the range of our thermal analysis. In contrast, the melting point of MoO_3 is 795 °C,

https://doi.org/10.1021/acs.iecr.1c02822
Ind. Eng. Chem. Res. 2021, 60, 13991−14003

much lower compared with that of Mo_2C, which may lead to detectable heat effects corresponding to phase transition of MoO_3 under FAU confinement at about 650 °C.

In Figure 7, we plotted the formation enthalpy of each Mo_2C/FAU from its constituent oxides and Mo_2C (ΔH_f) at 25

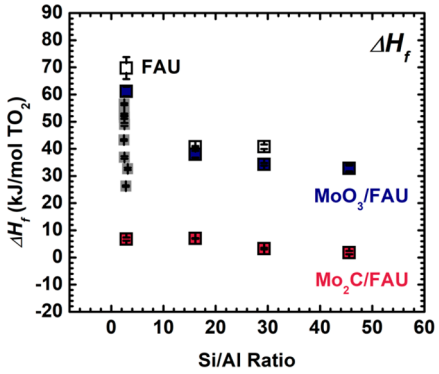

Figure 7. Enthalpies of formation of all Mo_2C/FAU samples from constituent oxides and carbides (SiO_2, Al_2O_3, Mo_2C, and H_2O) at 25 °C (per TO_2). The formation enthalpies of previously reported FAU[33] and MoO_3/FAU[33] samples by our group, and ion-exchanged zeolite Y by Yang and Navrotsky in 2000, are also plotted (gray squares) to elucidate the rich energetic landscape of guest−host systems based on FAU.[29]

°C, derived from the directly measured drop solution enthalpies (ΔH_{ds}) in molten lead borate at 700 °C using the thermodynamic cycle in Table 2. The drop solution enthalpies (ΔH_{ds}) for constituent oxides, Mo_2C, and water in molten lead borate at 700 °C and the formation enthalpies from elements ($\Delta H_{f,el}$) at 25 °C are listed in Table S1. The energetic contributions of hydration are corrected to 25 °C using the dehydration enthalpies ($\Delta H_{deh,l}$, see Table S2) derived using TG-DSC-MS. As Si/Al ratio increases, the ΔH_f of the Mo_2C/FAU tends to be slightly less endothermic, covering a narrow range spanning from ∼7.0 to ∼2.0 kJ/mol per TO_2. Here, "TO_2" denotes tetrahedron unit of framework silicon or aluminum, specifically, either SiO_2 or AlO_2^-. Such low ΔH_f magnitudes comparable to 0.0 kJ/mol TO_2 strongly suggest that the energetic states of Mo_2C/FAU samples are thermodynamically close to their corresponding dense phase assemblage of constituent oxides and carbide, including Al_2O_3, SiO_2 Mo_2C, and H_2O. Interestingly, it is noticed that at the same Si/Al ratio and Mo loading, ΔH_f of Mo_2C/FAU is much less endothermic than those of parent FAU and MoO_3/FAU, by more than ∼30.0 kJ/mol TO_2 (see Figure 7 and Table 3). In contrast, encapsulation of MoO_3 stabilizes the empty FAU, but, much less, by only ∼10.0 kJ/mol TO_2. Such a significant difference in ΔH_f between MoO_3/FAU and Mo_2C/FAU is because we used Mo_2C as the reactant in the thermodynamic cycle to derive ΔH_f of Mo_2C/FAU (Table 2), and Mo_2C has a very exothermic ΔH_{ds} under the oxidative environment within the calorimeter (see Table S1). Moreover, it is also possible that thermal decomposition of the free carbon, a common impurity on TMC/zeolites catalysts, may lead to more negative ΔH_{ds}. In general, $\Delta H_{f,el}$ of Mo_2C/FAU samples share the same trend as that of ΔH_f, and $\Delta H_{f,el}$ (Mo_2C/FAU) is also more exothermic than $\Delta H_{f,el}$ (MoO_3/FAU) at the same Si/Al ratio (see Table 3). Thus, the ΔH_f results suggest that at the same Mo loading, confinement of refractory Mo_2C is energetically more favorable than encapsulation of MoO_3 in the same zeolite Y host.

Surprisingly, although energetically favorable interfacial binding was expected, we were surprised to see that the calculated Mo_2C−FAU interaction enthalpy, ΔH_{inter} (Mo_2C/FAU, kJ/mol TO_2) is much more exothermic than ΔH_{inter} (MoO_3/FAU) at the same Si/Al and Mo loading. Specifically, we would like to highlight that the most exothermic ΔH_{inter} (Mo_2C/FAU), −76.5 ± 2.4 kJ/mol TO_2, is seen on Mo_2C/2.9FAU, which features the strongest Mo_2C−FAU interfacial bonding with high polarity, supported by the *in situ* DRIFS data (see Figures 4 and 5). All the other ΔH_{inter} of Mo_2C/FAU samples with higher Si content, are around −35 kJ/mol per TO_2. This moderately strong bonding is from a full spectrum of silanols (Si−OH) on the internal surface of FAU, which anchor the refractory Mo_2C particles, likely through covalent bonds. Although we have observed a similar trend on ΔH_{inter} (MoO_3/FAU), the magnitudes are entirely different, nearly an order of magnitude less exothermic. This is possible considering the multiple phase and/or redox transition events observed during thermal analysis of MoO_3/FAU, in which the subnano-MoO_3 particles, systematically and stepwise seek for lower energetic states to pay the "loan" for encapsulation by altering its local short- and/or long-range order details in the thermal synthesis processes.[33] In other words, the low melting point and flexible phase/redox transition behaviors of encapsulated MoO_3 reduce the total system energy leading to less exothermic MoO_3−FAU interfacial interactions. On the other hand, after initial dehydration, the "featureless" thermal analysis curves of Mo_2C/FAU samples, determined by its high melting point (2687 °C), strongly suggest that it is likely the robust Mo_2C−FAU interfacial bonding, not the phase or redox transition of Mo_2C guest species, governs the tight encapsulation of Mo_2C in zeolite Y, mirrored by the highly exothermic ΔH_{inter} (Mo_2C/FAU). Furthermore, it is possible

Table 2. Thermodynamic Cycle to Calculate the Enthalpies of Formation (per TO_2) at 25 °C of FAU and Mo_2C/FAU Samples from Their Constituent Oxides and Mo_2C, and Elements

$(MoC_{0.5})_x\cdot(SiO_2)_y\cdot(Al_2O_3)_z\cdot nH_2O_{(s,25°C)} + 2xO_{2(g,700°C)} \rightarrow xMoO_{3(soln.,700°C)} + ySiO_{2(soln.,700°C)} + zAl_2O_{3(soln.,700°C)} + 0.5xCO_{2\ (g,700°C)} + nH_2O_{(g,700°C)}$	$\Delta H_1 = \Delta H_{ds}$
$MoC_{0.5(s,25°C)} + 2O_{2(g,700°C)} \rightarrow MoO_{3(soln.,700°C)} + 0.5CO_{2(g,700°C)}$	ΔH_2
$SiO_{2(s,25°C)} \rightarrow SiO_{2(soln.,700°C)}$	ΔH_3
$Al_2O_{3(s,25°C)} \rightarrow Al_2O_{3(soln.,700°C)}$	ΔH_4
$H_2O_{(l,25°C)} \rightarrow H_2O_{(g,700°C)}$	ΔH_5
$Mo_{(s,25°C)} + 1/2C_{(s,25°C)} \rightarrow MoC_{0.5(s,25°C)}$	ΔH_6
$Si_{(s,25°C)} + O_{2(g,\ 25\ °C)} \rightarrow SiO_{2(s,25°C)}$	ΔH_7
$2Al_{(s,25°C)} + 3/2O_{2(g,25°C)} \rightarrow Al_2O_{3(s,25°C)}$	ΔH_8
$(MoC_{0.5})_x\cdot(SiO_2)_y\cdot(Al_2O_3)_z\cdot nH_2O_{(s,25°C)} \rightarrow (MoC_{0.5})_x\cdot(SiO_2)_y\cdot(Al_2O_3)_{z(s,25°C)} + nH_2O_{(l,25°C)}$	ΔH_9
$(MoC_{0.5})_x\cdot(SiO_2)_y\cdot(Al_2O_3)_{z(s,25°C)} + 2xO_{2(g,700°C)} \rightarrow xMoO_{3(soln.,700°C)} + ySiO_{2(soln.,700°C)} + zAl_2O_{3(soln.,700°C)} + 0.5xCO_{2(g,700°C)}$	$\Delta H_{10} = \Delta H_{ds,correct}$
$\Delta H_{ds,correct} = \Delta H_{10} = \Delta H_1 - n\Delta H_5 - \Delta H_9$	
$xMoC_{0.5(s,25°C)} + ySiO_{2(s,25°C)} + zAl_2O_{3(s,25°C)} \rightarrow (MoC_{0.5})_x\cdot(SiO_2)_y\cdot(Al_2O_3)_{z(s,25°C)}$	$\Delta H_{11} = \Delta H_f$
$\Delta H_f = \Delta H_{11} = x\Delta H_2 + y\Delta H_3 + z\Delta H_4 - \Delta H_{10}$	
$xMo_{(s,25°C)} + 1/2xC_{(s,25°C)} + ySi_{(s,25°C)} + 2zAl_{(s,25°C)} + (y + 3z/2)O_{2(g,25°C)} \rightarrow (MoC_{0.5})_x\cdot(SiO_2)_y\cdot(Al_2O_3)_{z(s,25°C)}$	$\Delta H_{12} = \Delta H_{f\text{-}el}$
$\Delta H_{f\text{-}el} = \Delta H_{12} = x\Delta H_6 + y\Delta H_7 + z\Delta H_8 + \Delta H_{11}$	
$xMoC_{0.5(s,25°C)} + (SiO_2)_y\cdot(Al_2O_3)_{z(s,25°C)} \rightarrow (MoC_{0.5})_x\cdot(SiO_2)_y\cdot(Al_2O_3)_{z(s,25°C)}$	$\Delta H_{13} = \Delta H_{inter}$
$\Delta H_{inter} = \Delta H_{13} = \Delta H_{12,MoC0.5/FAU} - \Delta H_{12,FAU} - x\Delta H_6$	

https://doi.org/10.1021/acs.iecr.1c02822
Ind. Eng. Chem. Res. 2021, 60, 13991−14003

Table 3. Enthalpies of Drop Solution (ΔH_{ds}) and Formation Enthalpies from Oxides and Carbides (ΔH_f), and Elements ($\Delta H_{f,el}$) at 25 °C (per TO_2) of All Samples, Including FAU, MoO_3/FAU, and Mo_2C/FAU[a]

sample	ΔH_{ds} (kJ/mol)	ΔH_f (kJ/mol)	$\Delta H_{f,el}$ (kJ/mol)	$\Delta H_{deh,l}$ (kJ/mol H_2O)	$\Delta H_{deh,l}$ [a] (kJ/mol H_2O)	ΔH_{inter} (kJ/mol)
2.9FAU	50.3 ± 4.0[33]	69.7 ± 4.1[33]	−822.1 ± 2.0[33]	67.9 ± 2.1[33]	14.9 ± 2.1[33]	N/A
16.1FAU	19.0 ± 0.3[33]	40.8 ± 0.3[33]	−865.7 ± 0.2[33]	97.0 ± 0.8[33]	30.9 ± 0.8[33]	N/A
29.3FAU	13.6 ± 0.8[33]	40.8 ± 0.8[33]	−867.5 ± 0.4[33]	109.8 ± 3.9[33]	37.7 ± 3.9[33]	N/A
45.6FAU	14.7 ± 1.1[33]	32.8 ± 1.1[33]	−871.9 ± 0.8[33]	176.1 ± 4.0[33]	88.9 ± 4.0[33]	N/A
MoO_3/2.9FAU	47.2 ± 1.7[33]	61.1 ± 1.8[33]	−849.1 ± 1.0[33]	75.6 ± 3.8[33]	21.3 ± 3.8[33]	−8.4 ± 2.6[33]
MoO_3/16.1FAU	20.8 ± 1.2[33]	38.0 ± 1.2[33]	−891.8 ± 0.6[33]	107.9 ± 1.7[33]	38.9 ± 1.7[33]	−3.0 ± 0.2[33]
MoO_3/29.3FAU	18.2 ± 0.5[33]	34.3 ± 0.5[33]	−894.2 ± 0.3[33]	99.4 ± 2.9[33]	26.4 ± 2.9[33]	−6.6 ± 0.1[33]
MoO_3/45.6FAU	17.0 ± 1.4[33]	32.8 ± 1.4[33]	−896.3 ± 0.7[33]	98.5 ± 3.9[33]	19.3 ± 3.9[33]	−4.3 ± 0.4[33]
Mo_2C/2.9FAU	83.1 ± 0.6	6.7 ± 0.6	−899.2 ± 1.3	86.9 ± 1.4	32.5 ± 1.4	−76.4 ± 2.4
Mo_2C/16.1FAU	29.4 ± 0.1	7.1 ± 0.1	−900.2 ± 0.6	180.6 ± 2.4	100.6 ± 2.4	−33.7 ± 0.6
Mo_2C/29.3FAU	26.2 ± 0.3	3.3 ± 0.3	−905.7 ± 0.5	139.2 ± 3.9	55.4 ± 3.9	−37.5 ± 0.6
Mo_2C/45.6FAU	26.7 ± 0.6	1.9 ± 0.6	−908.0 ± 0.7	130.8 ± 2.8	48.3 ± 2.8	−35.4 ± 1.1

[a]The dehydration enthalpy of each sample relative to liquid water ($\Delta H_{deh,l}$) at 25 °C and enthalpies of interactions (ΔH_{inter}) are also listed. Here, the dehydration enthalpies were calculated based on the thermodynamic cycle in Table S2.

that the reduced FAU lattice size (see Figure 1b) and restored surface hydroxyls in carburization (see Figure 3e−h), also contribute to ΔH_{inter} (Mo_2C/FAU) by applying enhanced confinement effects and stronger surface binding, respectively. Currently, we are working on identification of these intricate interfacial bonding and the exact Mo_2C local structures and assemblages in FAU at the atomic level using the synchrotron X-ray atomic pair distribution function (PDF). We will report those separately in future publications.

CONCLUSIONS

Here, we reported a systematic study on formation energetics of Mo_2C confinement in zeolite Y (Mo_2C/FAU) with various Si/Al ratios, in which high temperature oxide melt solution calorimetry was coupled with *in situ* DRIFTS and other fundamental structural, morphological, and thermal analyses. The results suggest that (i) Mo_2C/FAU formation from constituent oxides and Mo_2C (ΔH_f) is only slightly endothermic, ranging from ∼7.0 to ∼2.0 kJ/mol TO_2; (ii) encapsulation of Mo_2C is energetically more favorable compared with MoO_3 confinement in FAU; (iii) the physicochemical natures of the confined guest species also play critical roles in reducing the total energy of the system, and in governing the magnitudes of guest−host interfacial interactions, evidenced by the differences in phase and/or redox transitions of MoO_3 and Mo_2C under confinement, and reflected by ΔH_f and ΔH_{inter}. From a thermodynamic perspective, we anticipate that the fundamental knowledge enabled in this study will potentially benefit the chemical engineering society by providing quantitative benchmarking data for machine learning and simulation that may lead to predictive design, synthesis, and processing of supported heterogeneous catalytic materials from refractory transition metal carbides.

ASSOCIATED CONTENT

Supporting Information

The Supporting Information is available free of charge at https://pubs.acs.org/doi/10.1021/acs.iecr.1c02822.

Additional X-ray diffraction, DRIFTS, thermal analysis, and calorimetric data (PDF)

AUTHOR INFORMATION

Corresponding Author

Di Wu − *Alexandra Navrotsky Institute for Experimental Thermodynamics, The Gene and Linda Voiland School of Chemical Engineering and Bioengineering, Department of Chemistry, and Materials Science and Engineering, Washington State University, Pullman, Washington 99163, United States;* orcid.org/0000-0001-6879-321X; Email: d.wu@wsu.edu

Authors

Xianghui Zhang − *Alexandra Navrotsky Institute for Experimental Thermodynamics and The Gene and Linda Voiland School of Chemical Engineering and Bioengineering, Washington State University, Pullman, Washington 99163, United States*

Margaret E. Reece − *Alexandra Navrotsky Institute for Experimental Thermodynamics and Department of Chemistry, Washington State University, Pullman, Washington 99163, United States*

Cody B. Cockreham − *Alexandra Navrotsky Institute for Experimental Thermodynamics and The Gene and Linda Voiland School of Chemical Engineering and Bioengineering, Washington State University, Pullman, Washington 99163, United States; Earth and Environmental Sciences Division, Los Alamos National Laboratory, Los Alamos, New Mexico 87545, United States*

Hui Sun − *Petroleum Processing Research Center and International Joint Research Center of Green Energy Chemical Engineering, East China University of Science and Technology, Shanghai 200237, China;* orcid.org/0000-0002-8544-756X

Baodong Wang − *National Institute of Clean-and-Low-Carbon Energy, Beijing 102211, China*

Hongwu Xu − *Earth and Environmental Sciences Division, Los Alamos National Laboratory, Los Alamos, New Mexico 87545, United States*

Junming Sun − *The Gene and Linda Voiland School of Chemical Engineering and Bioengineering, Washington State University, Pullman, Washington 99163, United States;* orcid.org/0000-0002-0071-9635

Xiaofeng Guo − *Alexandra Navrotsky Institute for Experimental Thermodynamics, Department of Chemistry, and Materials Science and Engineering, Washington State*

University, Pullman, Washington 99163, United States; orcid.org/0000-0003-3129-493X

Ha Su − *The Gene and Linda Voiland School of Chemical Engineering and Bioengineering, Washington State University, Pullman, Washington 99163, United States*

Yong Wang − *The Gene and Linda Voiland School of Chemical Engineering and Bioengineering, Washington State University, Pullman, Washington 99163, United States; Institute for Integrated Catalysis, Pacific Northwest National Laboratory, Richland, Washington 99163, United States;* orcid.org/0000-0002-8460-7410

Complete contact information is available at: https://pubs.acs.org/10.1021/acs.iecr.1c02822

Notes

The authors declare no competing financial interest.

Biographies

Xianghui Zhang received his B.S. from Shangqiu Normal University, Henan, China, in 2012. He earned his M.E. in Chemical Engineering from Dalian University of Technology, Liaoning, China, in 2015. He is currently a Ph.D. candidate under the guidance of Professor Di Wu in the Alexandra Navrotsky Institute for Experimental Thermodynamics, and Professor Su Ha in the Gene and Linda Voiland School of Chemical Engineering and Bioengineering at Washington State University (WSU). His research is focused on structure−performance−thermodynamics relationships of porous materials and layered double hydroxides.

Margaret E. Reece obtained her B.S. in Chemistry from Ball State University, Muncie, Indiana in 2017. She began pursuing a Ph.D. at Washington State University (WSU) in analytical chemistry. After joining Professor Xiaofeng Guo's group, her research has included thermodynamic studies of rare earth and uranic nanominerals produced synthetically and biotically, as well as characterizing the environmental behavior of these species.

Cody B. Cockreham obtained his B.S. Degree in Chemical and Materials Engineering from New Mexico State University in the Spring of 2017. Following graduation, he began pursuing a Ph.D. at Washington State University (WSU) in the Alexandra Navrotsky Institute for Experimental Thermodynamics with Professor Di Wu's research group. Since 2018, Cody has held a Graduate Assistantship in the Earth and Environmental Sciences Division at Los Alamos National Laboratory under Senior Scientist Hongwu Xu. His research is focused on materials chemistry and thermodynamics of energy related materials including but not limited to 2D layered nanomaterials, kerogen-rich shales, and nuclear materials.

Hui Sun is a Professor in the School of Chemical Engineering at East China University of Science and Technology (ECUST), Shanghai, China. He received his B.S. in 2004 from Jiangnan University, and Ph.D. from ECUST in 2009. He worked in the Peter A. Rock Thermochemistry Laboratory and NEAT ORU at the University of California, Davis (UC Davis), as a Visiting Scholar from 2013 to 2014. His research interests include separation, purification. and conversion of energy sources, specifically, adsorption using porous framework structures, absorption involving functional solvents, and heterogeneous catalysis employing solid-state materials.

Baodong Wang is the CTO of National Institute of Clean-and-Low Carbon Energy (NICE), China Energy Group. He received his Ph.D in 2007 at University College London (UCL), United Kingdom (UK). He then went to University of Akron, Ohio for Postdoc. He spent three years as an Engineer R&D at Doosan Babcocks Energy at UK. He has served as the CTO at NICE in the field of environmental protection for more than 10 years.

Hongwu Xu is a Senior Scientist (Scientist 5) of the Earth and Environmental Sciences Division (EES) at Los Alamos National Laboratory, United States. His research involves structural characterization and thermodynamic measurements of natural minerals and synthetic materials, enabling determination of their structure−stability relationships at relevant pressure/temperature conditions. The systems he has studied include oxides, hydroxides, silicates, titanates, niobates, sulfates, gas hydrates, rare Earth and actinide compounds, with a wide range of Earth, energy, and environmental applications. He has expertise in high-pressure high-/low-temperature neutron and synchrotron X-ray scattering, electron microscopy, and various calorimetric techniques. He has a Ph.D. and a M.A. in Geosciences from Princeton University, United States, and a M.S. in Mineralogy and Crystallography and a B.S. in Mineralogy, Petrology, and Geochemistry from Nanjing University, China. He is a Fellow of the Mineralogical Society of America (MSA), currently serves as Editor-in-Chief for MSA's flagship journal, *American Mineralogist*, and has published about 200 papers in peer-reviewed journals in geology, chemistry, and materials science. In 2020, a mineral, Xuite, was named after him and his collaborator (Huifang Xu) in recognition of their contributions in mineral sciences.

Junming Sun is an Assistant Research and Major Professor in Professor Yong Wang's group at Washington State University (WSU), United States. He received his Ph.D. from Dalian Institute of Chemical Physics (DICP) of Chinese Academy of Science (CAS) in 2007 (Supervised by Professor Xinhe Bao), after which he worked with Professor Bruce C. Gates at UC Davis (2007−2008) and then with Professor Yong Wang at Pacific Northwest National Laboratory (2008−2011) as a Postdoctoral Researcher. His current research interests include fundamental understanding and rational design of acid−base/supported metal catalysts for biomass derived small oxygenates, bimetallic catalysts for hydrodeoxygenation.

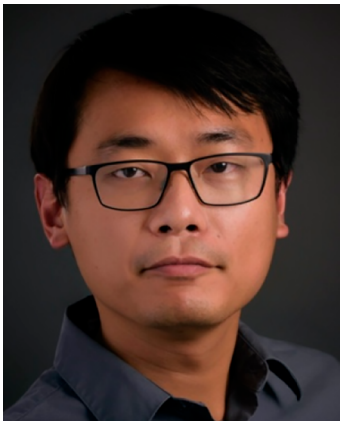

Xiaofeng Guo is an Assistant Professor of the Department of Chemistry and the Alexandra Navrotsky Institute for Experimental Thermodynamics at Washington State University (WSU). He got his Ph.D. in Chemistry from the University of California, Davis (UC Davis) in 2014 and was a G. T. Seaborg Postdoctoral Fellow at Los Alamos National Laboratory (2015−2017). His current research interests are thermodynamics of f-block solid-state systems, including nuclear fuels, wastes, and critical metal minerals, and their behaviors under high temperature and high pressure conditions.

https://doi.org/10.1021/acs.iecr.1c02822
Ind. Eng. Chem. Res. 2021, 60, 13991−14003

Su Ha is a Professor in the Gene and Linda Voiland School of Chemical Engineering and Bioengineering at Washington State University (WSU). He is also the Director for the O.H. Reaugh Laboratory for Oil and Gas Processing Research at WSU. He joined the school in 2005 as an Assistant Professor after completing his Ph.D. degree in chemical engineering from University of Illinois at Urbana−Champaign. He has published over 70 publications in the research areas of energy generations from alternative fuels. His researches have been cited over 5500 times with an h-index of 30. In 2014, he was named as a Highly Cited Researcher by Thomson Reuters. His researches focus on generating hydrogen gas from biofuels and abundant natural gases, developing fuel cells that directly convert the chemical energy of small organic molecules (e.g., formic acid) or logistic fuels (e.g., gasoline and biodiesel) to electrical power, working with natural enzymes to produce electrical power from sugars, and developing electric field-assisted fuel reforming systems.

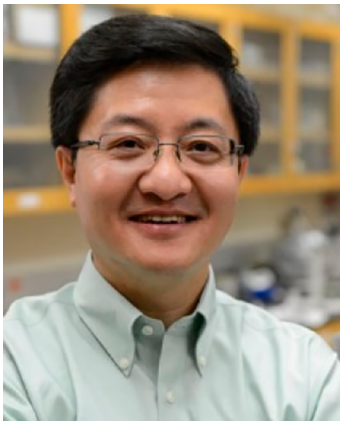

Yong Wang is the Voiland Distinguished Professor in Chemical Engineering at Washington State University (WSU) and a Laboratory Fellow and Associate Director of Institute for Integrated Catalysis at Pacific Northwest National Laboratory (PNNL). Dr. Wang received a Ph.D. degree in Chemical Engineering from WSU in 1993 and then joined PNNL in 1994 as a postdoc. He was promoted to laboratory Fellow in 2005. In 2009, Dr. Wang took a joint appointment at PNNL and WSU. Dr. Wang is best known for his leadership in the development of novel catalytic materials and reaction engineering to address the issues related to energy and atom efficiency related to the conversion of fossil and biomass feedstocks to fuels and chemicals. Dr. Wang has authored more than 360 peer-reviewed publications and is the inventor on 287 issued patents including 110 issued U.S. patents. He is a Fellow of AIChE (American Institute of Chemical Engineers), ACS (American Society of Chemistry), RSC (Royal Society of Chemistry), AAAS (American Association of the Advancement of Science), and NAI (National Academy of Inventors). He has won numerous awards including the 2021 ACS E. V. Murphree Award in Industrial Chemistry & Engineering, 2019 AIChE Catalysis and Reaction Engineering Practice Award, 2017 ACS I&EC Division Fellow Award, 2006 Asian American Engineer of the Year Award, Presidential Green Chemistry Award, 3 R&D 100 Awards, Distinguished Alumni Achievement Award from Chemical Engineering at WSU, 2 PNNL Inventor of the Year Awards, Battelle Distinguished Inventor Award, and the first recipient of PNNL Laboratory Director's Award for Exceptional Scientific Achievement Award. He is the past Chair of the ACS Energy & Fuel Division and Director to the AIChE Catalysis & Reaction Engineering Division, and currently serves Editorial Board Member of eight catalysis and energy related journals including *ACS Catalysis, JACS Au*, and *Catalysis Today*.

Di Wu is an Assistant Professor in the Gene and Linda Voiland School of Chemical Engineering and Bioengineering at Washington State University (WSU). He is also the Founding Director of the Alexandra Navrotsky Institute for Experimental Thermodynamics (AlexInstitute) and an affiliate faculty member in the Department of Chemistry, and Materials Science & Engineering Program at WSU. He earned his B.S. from Zhejiang University, China, in 2006, M.S. from the University of Akron in 2008, and Ph.D. from the University of California, Davis (UC Davis) under the guidance of Professor Alexandra Navrotsky, in 2012, all in Chemical Engineering. He was a Postdoctoral Fellow at the Peter A. Rock Thermochemistry Laboratory and NEAT ORU at UC Davis, from 2013 to 2016. His current research interests include experimental thermodynamics of materials employed in energy storage, heterogeneous catalysis, carbon capture and sequestration, and nanogeoscience. He also specializes in calorimetry technology development for *in situ* measurements. Dr. Wu currently serves as the Associate Editor of *American Mineralogist*, the flagship journal of the Mineralogical Society of America (MSA), and *International Journal of Ceramic Engineering and Science* (IJCES), an open access interdisciplinary journal of The American Ceramic Society (ACerS). He is also the Editorial Board Member of *Chemical Thermodynamics and Thermal Analysis* (CTTA) and *Advanced Composites and Hybrid Materials* (ACHM).

■ ACKNOWLEDGMENTS

Di Wu thanks Profs. Alexandra Navrotsky, Bruce C. Gates, Stacey I. Zones, Gang-yu Liu, Ricardo H. R. Castro, and Roland Faller for their guidance during his Ph.D. education and postdoctoral training. Di Wu also thanks Prof. James N. Petersen and the WSU colleagues for the exceptionally strong support during his junior faculty stage. This work was supported by institutional funds from the Gene and Linda Voiland School of Chemical Engineering and Bioengineering and Alexandra Navrotsky Institute for Experimental Thermo-

https://doi.org/10.1021/acs.iecr.1c02822
Ind. Eng. Chem. Res. 2021, 60, 13991−14003

dynamics at Washington State University. Xianghui Zhang was supported by Chambroad Distinguished Scholarship. Cody B. Cockreham received support from the Achievement Rewards for College Scientists (ARCS) Fellowship from the ARCS Seattle Chapter. Margaret E. Reece and Xiaofeng Guo acknowledge the support by the institutional funds from the Department of Chemistry and the U.S. Department of Energy, Office of Nuclear Energy, Grant DE-NE0008582. Portions of this research were also supported by collaboration, services, and infrastructure through the Nuclear Science Center User Facility at WSU. Hui Sun acknowledges the financial support from the National Natural Science Foundation of China, Grants 21878097 and 91634112, and the Natural Science Foundation of Shanghai, Grant 21ZR1417700. We also thank Dr. Renqin Zhang for discussions and suggestions.

REFERENCES

(1) Vogt, E. T. C.; Weckhuysen, B. M. Fluid Catalytic Cracking: Recent Developments on the Grand Old Lady of Zeolite Catalysis. *Chem. Soc. Rev.* **2015**, *44*, 7342−7370.
(2) Blay, V.; Louis, B.; Miravalles, R.; Yokoi, T.; Peccatiello, K. A.; Clough, M.; Yilmaz, B. Engineering Zeolites for Catalytic Cracking to Light Olefins. *ACS Catal.* **2017**, *7*, 6542−6566.
(3) Shi, Y.; Xing, E.; Wu, K.; Wang, J.; Yang, M.; Wu, Y. Recent Progress on Upgrading of Bio-Oil to Hydrocarbons over Metal/Zeolite Bifunctional Catalysts Yanchun. *Catal. Sci. Technol.* **2017**, *7*, 2385−2415.
(4) Ennaert, T.; Van Aelst, J.; Dijkmans, J.; De Clercq, R.; Schutyser, W.; Dusselier, M.; Verboekend, D.; Sels, B. F. Potential and Challenges of Zeolite Chemistry in the Catalytic Conversion of Biomass. *Chem. Soc. Rev.* **2016**, *45*, 584−611.
(5) Taarning, E.; Osmundsen, C. M.; Yang, X.; Voss, B.; Andersen, I.; Christensen, C. H. Zeolite-Catalyzed Biomass Conversion to Fuels and Chemicals. *Energy Environ. Sci.* **2011**, *4*, 793−804.
(6) Zahidi, E. M.; Oudghiri-hassani, H.; Mcbreen, P. H. Formation of Thermally Stable Alkylidene Layers on a Catalytically Active Surface. *Nature* **2001**, *409*, 1023−1026.
(7) Levy, R. B.; Boudart, M. Platinum-Like Behavior of Tungsten Carbide in Surface Catalysis. *Science* **1973**, *181*, 547−549.
(8) Iida, T.; Shetty, M.; Murugappan, K.; Wang, Z.; Ohara, K.; Wakihara, T.; Román-Leshkov, Y. Encapsulation of Molybdenum Carbide Nanoclusters inside Zeolite Micropores Enables Synergistic Bifunctional Catalysis for Anisole Hydrodeoxygenation. *ACS Catal.* **2017**, *7* (12), 8147−8151.
(9) Yang, C.; Lu, H.; Shi, Y.; Zhu, Y.; Wu, K.; Liu, Y.; Liu, C.; Liang, B. Nano Molybdenum Carbides Supported on Porous Zeolites for Kraft Lignin Decomposition to Aromatic Monomers in Ethanol. *Bioresour. Technol. Reports* **2020**, *11* (June), 100484.
(10) Ardakani, S. J.; Liu, X.; Smith, K. J. Hydrogenation and Ring Opening of Naphthalene on Bulk and Supported Mo_2C Catalysts. *Appl. Catal., A* **2007**, *324*, 9−19.
(11) Liu, X.; Ardakani, S. J.; Smith, K. J. The Effect of Mg and K Addition to a Mo_2C/HY Catalyst for the Hydrogenation and Ring Opening of Naphthalene. *Catal. Commun.* **2011**, *12* (6), 454−458.
(12) Kosinov, N.; Coumans, F. J. A. G.; Uslamin, E. A.; Wijpkema, A. S. G.; Mezari, B.; Hensen, E. J. M. Methane Dehydroaromatization by Mo/HZSM-5: Mono- or Bifunctional Catalysis? *ACS Catal.* **2017**, *7* (1), 520−529.
(13) Lezcano-González, I.; Oord, R.; Rovezzi, M.; Glatzel, P.; Botchway, S. W.; Weckhuysen, B. M.; Beale, A. M. Molybdenum Speciation and Its Impact on Catalytic Activity during Methane Dehydroaromatization in Zeolite ZSM-5 as Revealed by Operando X-Ray Methods. *Angew. Chem., Int. Ed.* **2016**, *55* (17), 5215−5219.
(14) Spivey, J. J.; Hutchings, G. Catalytic Aromatization of Methane. *Chem. Soc. Rev.* **2014**, *43*, 792−803.
(15) Majhi, S.; Mohanty, P.; Wang, H.; Pant, K.K. Direct Conversion of Natural Gas to Higher Hydrocarbons : A Review. *J. Energy Chem.* **2013**, *22* (4), 543−554.
(16) Zheng, Y.; Tang, Y.; Gallagher, J. R.; Gao, J.; Miller, J. T.; Wachs, I. E.; Podkolzin, S. G. Molybdenum Oxide, Oxycarbide, and Carbide: Controlling the Dynamic Composition, Size, and Catalytic Activity of Zeolite-Supported Nanostructures. *J. Phys. Chem. C* **2019**, *123* (36), 22281−22292.
(17) Gao, J.; Zheng, Y.; Fitzgerald, G. B.; De Joannis, J.; Tang, Y.; Wachs, I. E.; Podkolzin, S. G. Structure of Mo_2C_x and Mo_4C_x Molybdenum Carbide Nanoparticles and Their Anchoring Sites on ZSM-5 Zeolites. *J. Phys. Chem. C* **2014**, *118* (9), 4670−4679.
(18) Piccione, P. M.; Laberty, C.; Yang, S.; Camblor, M. A.; Navrotsky, A.; Davis, M. E. Thermochemistry of Pure-Silica Zeolites. *J. Phys. Chem. B* **2000**, *104*, 10001−10011.
(19) Petrovic, I.; Navrotsky, A. Thermochemistry of Na-Faujasites with Varying Si/Al Ratios. *Microporous Mater.* **1997**, *9*, 1−12.
(20) Navrotsky, A.; Trofymluk, O.; Levchenko, A. A. Thermochemistry of Microporous and Mesoporous Materials. *Chem. Rev.* **2009**, *109*, 3885−3902.
(21) Petrovic, I.; Navrotsky, A.; Davis, M. E.; Zones, S. I. Thermochemical Study of the Stability of Frameworks in High Silica Zeolites. *Chem. Mater.* **1993**, *5*, 1805−1813.
(22) Hu, Y.; Navrotsky, A.; Chen, C.; Davis, M. E. Thermochemical Study of the Relative Stability of Dense and Microporous Aluminophosphate Frameworks. *Chem. Mater.* **1995**, *7*, 1816−1823.
(23) Yang, S.; Navrotsky, A.; Phillips, B. L. *In Situ* Calorimetric, Structural, and Compositional Study of Zeolite Synthesis in the System $5.15Na_2O$-$1.00Al_2O_3$-$3.28SiO_2$-$165H_2O$. *J. Phys. Chem. B* **2000**, *104*, 6071−6080.
(24) Sun, H.; Wu, D.; Liu, K.; Guo, X.; Navrotsky, A. Energetics of Alkali and Alkaline Earth Ion-Exchanged Zeolite A. *J. Phys. Chem. C* **2016**, *120*, 15251−15256.
(25) Sun, H.; Wu, D.; Guo, X.; Navrotsky, A. Energetics and Structural Evolution of Na−Ca Exchanged Zeolite A during Heating. *Phys. Chem. Chem. Phys.* **2015**, *17*, 9241−9247.
(26) Piccione, P. M.; Yang, S.; Navrotsky, A.; Davis, M. E. Thermodynamics of Pure-Silica Molecular Sieve Synthesis. *J. Phys. Chem. B* **2002**, *106*, 3629−3638.
(27) Wu, D.; Hwang, S.; Zones, S. I.; Navrotsky, A. Guest−Host Interactions of a Rigid Organic Molecule in Porous Silica Frameworks. *Proc. Natl. Acad. Sci. U. S. A.* **2014**, *111*, 1720−1725.
(28) Zones, S. I.; Jayanthi, K.; Pascual, J.; Xie, D.; Navrotsky, A. Energetics of the Local Environment of Structure-Directing Agents In Fl Uence Zeolite Synthesis. *Chem. Mater.* **2021**, *33*, 2126−2138.
(29) Yang, S.; Navrotsky, A. Energetics of Formation and Hydration of Ion-Exchanged Zeolite Y. *Microporous Mesoporous Mater.* **2000**, *37*, 175−186.
(30) Sun, H.; Wu, D.; Guo, X.; Shen, B.; Liu, J.; Navrotsky, A. Energetics of Con Fi Nement of N-Hexane in Ca−Na Ion Exchanged Zeolite A. *J. Phys. Chem. C* **2014**, *118*, 25590−25596.
(31) Yang, S.; Guo, X.; Verma, A.; Shiflett, M. B.; Corbin, D. R.; Navrotsky, A. Thermochemical Insights into Stability and Hydration of Ion- Exchanged Zeolite ZK-5 (KFI Framework). *J. Phys. Chem. C* **2020**, *5*, 26193−26202.
(32) Zhang, X.; Cockreham, C. B.; Huang, Z.; Sun, H.; Yang, C.; Marin-Flores, O. G.; Wang, B.; Guo, X.; Ha, S.; Xu, H.; Wu, D. Thermodynamics of Water-Cationic Species-Framework Guest-Host Interactions within Transition Metal Ion-Exchanged Mordenite Relevant to Selective Anaerobic Oxidation of Methane to Methanol. *J. Phys. Chem. Lett.* **2020**, *11* (12), 4774−4784.
(33) Zhang, X.; Strzelecki, A. C.; Goncharov, V.; Cockreham, C. B.; Li, H.; Sun, J.; Guo, X.; Xu, H.; Ha, S.; Wang, B.; Wang, Y.; Wu, D. Thermodynamics of Molybdenum Trioxide (MoO_3) Encapsulated in Zeolite Y. *Authorea* **2021**, 1−16, DOI: 10.22541/au.162206667.74058496/v1.
(34) Zhang, X.; Chaudhary, N.; Hawkins, M. R.; Cockreham, C. B.; Yang, C.; Shangguan, J.; Hensley, A. J. R.; Chin, Y. C.; Ha, S.; Mcewen, J.; Wu, D. Determining the Hydration Energetics on

Carbon-Supported Ru Catalysts : An Adsorption Calorimetry and Density Functional Theory Study. *Catal. Today* **2021**, *365*, 172−180.
(35) Solymosi, F.; Széchenyi, A. Aromatization of N-Butane and 1-Butene over Supported Mo_2C Catalyst. *J. Catal.* **2004**, *223* (1), 221−231.
(36) Sheng, H.; Schreiner, E. P.; Zheng, W.; Lobo, R. F. Non-Oxidative Coupling of Methane to Ethylene Using Mo_2C/[B]ZSM-5. *ChemPhysChem* **2018**, *19* (4), 504−511.
(37) Navrotsky, A. Progress and New Directions in Calorimetry: A 2014 Perspective. *J. Am. Ceram. Soc.* **2014**, *97* (11), 3349−3359.
(38) Gao, J.; Zheng, Y.; Jehng, J.-M.; Tang, Y.; Wachs, I. E.; Podkolzin, S. G. Identification of molybdenum Oxide Nanostructures on Zeolites for Natural Gas Conversion. *Science* **2015**, *348*, 686−690.
(39) Omegna, A.; Vasic, M.; Van Bokhoven, J. A.; Pirngruber, G.; Prins, R. Dealumination and Realumination of Microcrystalline Zeolite Beta: An XRD, FTIR and Quantitative Multinuclear (MQ) MAS NMR Study. *Phys. Chem. Chem. Phys.* **2004**, *6* (2), 447−452.
(40) Senderov, E.; Halasz, I.; Olson, D. H. On Existence of Hydroxyl Nests in Acid Dealuminated Zeolite Y. *Microporous Mesoporous Mater.* **2014**, *186*, 94−100.
(41) Ding, W.; Li, S.; Meitzner, G. D.; Iglesia, E. Methane Conversion to Aromatics on Mo/H-ZSM-5: Structure of Molybdenum Species in Working Catalysts. *J. Phys. Chem. B* **2001**, *105* (2), 506−513.
(42) Tempelman, C. H. L.; Hensen, E. J. M. On the Deactivation of Mo/HZSM-5 in the Methane Dehydroaromatization Reaction. *Appl. Catal., B* **2015**, *176*−*177*, 731−739.
(43) Matus, E. V.; Ismagilov, I. Z.; Sukhova, O. B.; Zaikovskii, V. I.; Tsikoza, L. T.; Ismagilov, Z. R.; Moulijn, J. A. Study of Methane Dehydroaromatization on Impregnated Mo/ZSM-5 Catalysts and Characterization of Nanostructured Molybdenum Phases and Carbonaceous Deposits. *Ind. Eng. Chem. Res.* **2007**, *46* (12), 4063−4074.
(44) Wu, W.; Wu, Z.; Liang, C.; Chen, X.; Ying, P.; Li, C. *In Situ* FT-IR Spectroscopic Studies of CO Adsorption on Fresh Mo_2C/Al_2O_3 Catalyst. *J. Phys. Chem. B* **2003**, *107* (29), 7088−7094.

NOTE ADDED AFTER ASAP PUBLICATION

This paper was originally published ASAP on September 17, 2021. Due to a production error, the TOC graphic and Figure 1 were rendered incorrectly. The revised version was reposted on September 17, 2021.

https://doi.org/10.1021/acs.iecr.1c02822
Ind. Eng. Chem. Res. 2021, 60, 13991−14003